ACS APPLIED POLYMER MATERIALS

pubs.acs.org/acsapm Article

Viscoelastic Characterization of Poly(3-hexylthiophene): Determination of Young's Modulus

Branston E. Mefferd, Visakhan V. Nambiar, Hongbing Lu, and Mihaela C. Stefan*

Cite This: ACS Appl. Polym. Mater. 2023, 5, 6318−6324 Read Online

ACCESS | Metrics & More | Article Recommendations | Supporting Information

ABSTRACT: Nanoindentation is an optimal technique for the measurement of thin film mechanical properties. Polymers present a unique problem in that their response to loading is time-dependent. Due to this, many of the most common nanoindentation methods are not suitable for probing polymer nanoscale properties. Despite this issue being well-known for decades, poly(3-hexylthiophene) has been exclusively analyzed by time-independent mechanical properties testing methods. Herein, we present a nanoindentation technique that analyzes the materials' time-dependent response under both constant rate loading and step loading. By determining viscoelastic functions, we are able to extract the Young's relaxation modulus of poly(3-hexylthiophene). The average Young's modulus acquired from viscoelastic nanoindentation is determined to be 260 ± 27 MPa. These results are in excellent agreement with specialized mechanical tests for thin films and show promise for the analysis of other organic semiconducting materials.

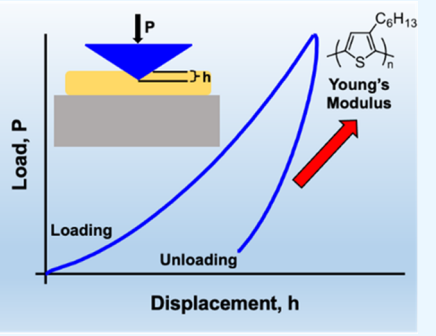

KEYWORDS: *organic semiconductor, mechanical properties, nanoindentation, Young's modulus, polymer film, viscoelasticity*

1. INTRODUCTION

Organic semiconductors (OSCs) are a promising alternative to silicon for use in optoelectronic devices, specifically for flexible electronics such as transistors, solar cells, and light-emitting diodes.[1−4] Such devices are multilayered, and the mechanical robustness of the layers within is directly related to their stability and performance.[5−7] Precise measurements of mechanical properties must be taken such that materials may be screened for a desired application. Considering the lower efficiency and stability of organic electronics to the inorganic counterparts, these materials are best suited for niche applications such as stretchable and flexible electronics.[5,6] Because of this, stretchability, elasticity, and adhesion are important qualities to be screened in order to make an optimized device. This presents a need for a characterization technique for screening materials and routine quality control. One difficulty that arises for mechanical testing is that organic semiconductors require solution processing. This often makes sample preparation impossible for traditional mechanical tests such as tensile tests.[8]

In addition, the organic semiconductor layer is prepared as a thin film, which behaves differently from the bulk material.[9] Several alternative methods for probing nanoscale mechanical properties have been presented, including specialized tensile testing through the film-on-water (FoW) and film-on-elastomer (FoE) techniques, continuous buckling, and nanoindentation.[5] The specialized tensile tests and continuous buckling method involve a tedious sample preparation process and require an operator to be present during testing. Nanoindentation is a highly effective technique for the characterization of the mechanical behavior of thin films while also possessing simple sample preparation and the ability for high throughput automation.

Nanoindentation has been largely utilized in determining mechanical properties such as Young's modulus, hardness, yield strength, and adhesion of linearly elastic materials.[10−13] The most commonly employed nanoindentation technique is the Oliver−Pharr method, which operates on the assumption of deformation lying within the linearly elastic range with the unloading portion of the load−displacement curve.[10]

For a Berkovich indenter tip, the tip cross-sectional area, $A(h)$, as a function of indentation depth, h, in nanometers, is given as,

$$A(h) = 24.66h^2 + 150h \tag{1}$$

the unloading stiffness is given as

$$S = \frac{dP}{dh} \tag{2}$$

the reduced modulus, E_r, is then calculated by

Received: May 5, 2023
Accepted: June 26, 2023
Published: July 11, 2023

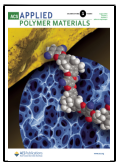

https://doi.org/10.1021/acsapm.3c00939
ACS Appl. Polym. Mater. 2023, 5, 6318−6324

$$E_r = \frac{S\sqrt{\pi}}{2\sqrt{A(h)}} \tag{3}$$

Young's modulus of the test specimen is determined by

$$\frac{1}{E_r} = \frac{(1-\nu_i^2)}{E_i} + \frac{(1-\nu_s^2)}{E_s} \tag{4}$$

where E_i and ν_i are the indenter modulus and Poisson's ratio, respectively, and E_s and ν_s are the sample's modulus and sample's Poisson's ratio.

Polymers exhibit a time-dependent response to loading due to viscoelastic behavior.[14] This is seen in a nanoindentation experiment through continuous deformation at a constant load or exhibition of a "nose" at the beginning of unloading. While the Oliver–Pharr method is acceptable for the analysis of time-independent materials, it does not adequately capture the time-dependent response seen in polymers, which often leads to an overestimation of Young's modulus.[15] Despite the lack of suitability utilizing the Oliver–Pharr technique on polymers, poly(3-hexylthiophene) (P3HT) (Figure 1), arguably the most well-studied semiconducting polymer, has been exclusively analyzed by this technique.

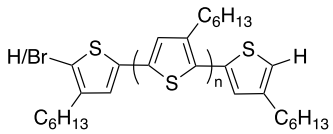

Figure 1. Head-to-tail coupled P3HT.

The first five rows in Table 1 present a compilation of Young's modulus values of P3HT determined through the Oliver–Pharr method. These values are in contrast to the data reported using film-on-water tensile testing as well as the continuous buckling method, which are also given in Tables 1 and S3.[21−26] Also listed in the last row is the Young's modulus obtained by viscoelastic nanoindentation in this paper; the details on the analysis will be provided in the sequel.

Table 1. P3HT Evaluated by the Oliver–Pharr Procedure

Young's modulus (GPa)	reference
42.2	Li et al. 16,
5.30–7.90	Nanayakkara et al. 17,
1.76	Pulliam et al. 18,
0.120	Gao et al. 19,
15.0–18.7	An et al. 20,
0.261–0.287[a]	Kim et al. 21,; Rodriquez et al. 22,
0.220–0.252[b]	O'Connor et al. 23,; Awartani et al. 24,
0.260[c]	Mefferd et al.

[a]Determined by the film-on-water tensile test. [b]Determined by the continuous buckling method. [c]This study, details on obtaining the data will be explained in Section 3.

While nanoindentation clearly lacks a consensus value to assign to P3HT, the continuous buckling and film-on-water technique are in good agreement with one another. The lack of accuracy and precision between independent nanoindentation tests demonstrates the need for a technique that can account for the time-dependent response that will be exhibited by semiconducting polymers. A method developed by Lu et al.[15] in 2003 involves measuring a material's creep compliance through the load–depth relationship acquired during a traditional nanoindentation test. The relaxation modulus is then acquired from an interconversion of the compliance, from which one may extract Young's relaxation modulus. The following sections give this procedure in detail.

1.1. Ramp Loading. First, we consider the nanoindentation on a homogeneous, isotropic, linearly viscoelastic half-space by a Berkovich indenter tip under constant rate loading. The indentation load–depth relationship is given by $P(t) = \dot{P}_o t H(t)$, where $\dot{P}_o$ is the loading rate and $H(t)$ is the Heaviside unit step function. Utilizing these parameters and considering a Lee and Radok's technique for time-dependent indentation under a prescribed loading history, indentation depth can be written as[15]

$$h^2(t) = \frac{\pi(1-\nu)\tan\alpha}{4}\left[\left(J_o + \sum_{i=1}^{N} J_i\right)t - \sum_{i=1}^{N} J_i\tau_i(1-e^{-t/\tau_i})\right] \tag{5}$$

where ν is Poisson's ratio, which is assumed to be constant, α is the angle generated between the cone generator of the indenter tip and substrate plane, J_o and J_i ($i = 1, 2, \cdots, N$) are shear creep coefficients, and τ_i ($i = 1, 2, \cdots, N$) are retardation times[27] eq 5 is then used to fit the experimental load–displacement data to determine the shear creep coefficients and retardation times for constructing the creep function based on the generalized Maxwell model given by the below Prony series.

$$J(t) = J_o + \sum_{i=1}^{N} J_i\tau_i(1-e^{-t/\tau_i}) \tag{6}$$

where $J(t)$ is the shear creep compliance function. Interconversion of the creep compliance to relaxation is accomplished via a numerical approach to yield the following shear relaxation function, $G(t)$.

$$G(t) = G_\infty + \sum_{i=1}^{N} G_i\tau_i(1-e^{-t/\tau_i}) \tag{7}$$

where $G(t)$ is the shear relaxation modulus, G_∞ and G_i ($i = 1, 2, \cdots, N$) are relaxation coefficients, and λ_i ($i = 1, 2, \cdots, N$) are relaxation times. The shear relaxation modulus is then converted to Young's relaxation modulus, $E(t)$, by the following relation

$$E(t) = 2G(t)(1+\nu) \tag{8}$$

from $E(t)$ to Young's modulus, E, at a constant strain rate, $\dot{\varepsilon}$[28,29]

$$E(\dot{\varepsilon}) = E_\infty + \sum_{i=1}^{N} E_i\frac{\tau_i\dot{\varepsilon}}{\varepsilon_o}(1-e^{-\varepsilon_o/\tau_i\dot{\varepsilon}}) \tag{9}$$

where the steady-state value, E_∞, is taken as Young's modulus.

1.2. Step Loading. Next, we consider nanoindentation under a step-loading history. A load is suddenly applied and can be represented by $P(t) = P_o H(t)$, where P_o is the holding load. The load–depth to creep relationship is given by the following formula

https://doi.org/10.1021/acsapm.3c00939
ACS Appl. Polym. Mater. 2023, 5, 6318−6324

$$J(t) = \frac{4h^2(t)}{\pi(1-\nu)P_o \tan \alpha} \quad (10)$$

By fitting the experimental load−displacement curve to the above equation, the shear creep function is obtained. The remainder of this procedure is analogous to ramp loading. The shear relaxation modulus is obtained from a numerical interconversion using creep compliance. Young's relaxation modulus is then extracted from the shear relaxation modulus, from which Young's modulus at a given loading rate is obtained.

2. EXPERIMENTAL ASPECTS

2.1. Materials. Hexylmagnesium bromide (Sigma-Aldrich, 2 M), dichloro(1,3-bis(diphenylphosphino)propane)nickel (TCI America, >98%), 3-bromothiophene (Fisher Chemical, >97%), *N*-bromosuccinimide (99%, Thermo Scientific Chemicals), Isopropylmagnesium chloride (Sigma-Aldrich, 2 M), and anhydrous diethyl ether (Fisher Chemical, laboratory grade) were all used as received. Tetrahydrofuran (Fisher Chemical, >99.7%) was dried using 3 Å molecular sieves for two days prior to use. Undoped silicon wafers were obtained from University Wafer. Chloroform (Sigma-Aldrich, >99%), toluene (Alfa Aesar, >99%), and dichlorobenzene (Sigma-Aldrich, >99%), concentrated sulfuric acid (Fisher Chemical, 96.5 wt %), and hydrogen peroxide (Sigma-Aldrich, 30 wt %) were all used as received. P3HT was synthesized via the Grignard metathesis method, which is detailed in the Supporting Information (SI).[30,31]

2.2. Material Characterization. A 500 MHz Bruker AVANCE III spectrometer was used in order to obtain ^{1}H NMR spectra for confirmation of molecular structure and degree of regioregularity. The polymer's molecular weight was determined by size exclusion chromatography on a Viscotec VE 3580 chromatograph with a CLM3009 column paired with a UV detector with a 254 nm laser source. The detector was calibrated to a polystyrene standard, and all experiments utilized THF as the mobile phase (1.0 mL/min flow rate). Digital scanning calorimetry was performed on a TA Instruments digital scanning calorimeter. Three cycles were conducted from 0 to 260 °C at a rate of 10 °C/min. The melting (T_m) and crystallizing temperatures (T_c) of P3HT were reported from cycle two. Atomic force microscopy (AFM) images were recorded on an Oxford Asylum Research Jupiter XR atomic force microscope in order to determine the surface roughness of films. The AFM was operated in tapping mode with a spring constant of 40 N/m and a scanning frequency of 0.75 MHz over a 10 × 10 μm^2 area. Film thickness was measured using an XP-1 Ambios Technology mechanical profilometer at a stylus force of 0.05 mg over a scan length of 2.0 mm at a scan rate of 0.05 mm/s. Scanning electron microscopy (SEM) images of the nanoindenter tip were acquired on a Zeiss Sigma 500VP scanning electron microscope with a secondary electron detector. Images were captured at an acceleration voltage of 7.00 kV at a working distance of 15.8 mm.

2.3. Sample Preparation. A detailed synthetic procedure for P3HT is given within the Supporting Information. The initial challenge for getting reliable nanoindentation data included ensuring sample preparation yielded films of suitable thickness and minimal surface roughness. Nanoindentation data can be unreliable at small penetration depths (≤100 nm), which can arise from surface roughness, sink-in effects, and pile-up effects.[15,32−34] In addition, it has been demonstrated that indentation depths that exceed 10% of the film thickness may observe the substrate effect, which would lead to an overestimation of the material's modulus.[35] In order to avoid these issues, films should be on the order of several microns thick. In this study, two casting methods and three solvents were screened for the preparation of thin films. All solutions were prepared by dissolving P3HT at a concentration of 25 mg/mL in chloroform, toluene, and dichlorobenzene. The P3HT solution was either drop cast or spin-coated onto silicon wafers previously treated with Piranha solution, followed by washes of deionized water, acetone, and isopropyl alcohol. All films were allowed to dry overnight before taking thickness and roughness measurements. The only films with sufficient quality for nanoindentation were cast from dichlorobenzene. These films were measured to be 7.9 μm thick with a root mean square surface roughness of 14.0 nm. The results of the thin film optimization are compiled in the Supporting Information.

2.4. Nanoindentation Experiments. An Agilent G200 Nano Indenter system was used for all nanoindentation tests. The G200 can reach a maximum load of 500 mN and a maximum depth >500 μm, with resolutions of ±50 nN and <0.01 nm, respectively. All nanoindentation experiments were performed at room temperature. Prior to each experiment, the instrument was allowed to equilibrate in an effort to minimize thermal drift. The allowable drift rate for these experiments was set to 0.05 nm/s. Over the course of a 100-second test, as in the step-loading experiment, this would equate to a maximum drift of ±5 nm, which is less than 1% of the indentation depth in all tests.

The Berkovich nanoindenter tip used in this study was made of diamond, and its geometry is shown in the supporting information, Figure S6. Calibration using fused silica is given in the Supporting Information. The Berkovich nanoindenter tip is modeled as an axisymmetric conical indenter that possesses a cone angle such that the area-to-depth relationship is the same as the actual pyramidal tip. The modeled conical indenter possesses a half-cone angle of 70.3°, which corresponds to α = 19.7°. For ramp-loading experiments, five loading rates were selected, spanning over an order of magnitude, from 0.05 to 1.0 mN/s. The step-loading experiments were carried out such that the holding load and resulting total penetration depth did not exceed 10% of the film thickness.

3. RESULTS AND DISCUSSION

3.1. P3HT Characterization. In the analysis of semiconducting polymers, it has been shown that mechanical properties have a dependency on molecular weight, regioregularity (RR%), degree of crystallinity, and morphology.[21,23,24,36] Due to this, it is imperative to match the chemical properties of the previous mechanical property studies conducted on P3HT. A detailed comparison of molecular weights, regioregularity, PDI, casting solvent, and strain rate (FoW only) is given in Table S3 of the supporting information. It should be noted that even amongst the continuous buckling and FoW techniques, there is not a perfect agreement for the elastic modulus of P3HT. This is likely due to large variations in the molecular weight and PDI. It has been shown that the elastic modulus of P3HT saturates at a value of about 250 MPa when possessing a molecular weight greater than 35 kg/mol. This has been deemed the point at which the polymer chains begin to entangle and has been shown to decrease the stiffness of the material.[22,23,25] This effect is also important regarding the thickness of films due to the confinement of polymer chains. Films possessing thickness >20 nm do not experience the confinement effect as the chains do not self-entangle, leading to measured elastic modulus values that are independent of the film thickness above this critical value.[25] It has been demonstrated that polymers with broad a PDI experience a plasticizing effect caused by the shorter length chains interacting with the longer chains that causes an increase in free volume, thus enhancing the chain mobility.[37,38] Due to these factors, careful consideration has been undertaken to compare the results of this work to those reported in the literature.

^{1}H NMR was performed on P3HT to determine the extent of head-to-tail linkages as well as absolute molecular weight, both of which are summarized in Table S1 and Figure S4 in the supporting information.[39] Size exclusion chromatography was used to determine the molecular weight and polydispersity

https://doi.org/10.1021/acsapm.3c00939
ACS Appl. Polym. Mater. 2023, 5, 6318−6324

index of P3HT, which were found to be 59 kg/mol and 1.54, respectively. These results are summarized in Table S1 and demonstrate great chemical similarity to the P3HT used in previous works.[22−24]

A differential thermogram was obtained from DSC analysis and is given in Figure S5. The crystallization temperature and melting temperature were determined to be 209 °C (T_c = 209 °C) and 240 °C (T_m = 240 °C), respectively. The melting enthalpy of the P3HT used in this study was calculated as 15.3 J/g (ΔH_m = 15.3 J/g), and an ideal P3HT crystallite possesses a melting enthalpy of 37.0 J/g (ΔH_m = 37.0 J/g).[33] By taking the ratio of these values, the degree of crystallinity was found to be 41.3%, which is also in a good agreement with previous studies.[21,40,41]

3.2. Nanoindentation by the Oliver−Pharr Method. To further elucidate the inability of the Oliver−Pharr method to analyze time-dependent materials accurately, we subjected our load−displacement curves to eqs 1−4. Figure 2 shows a

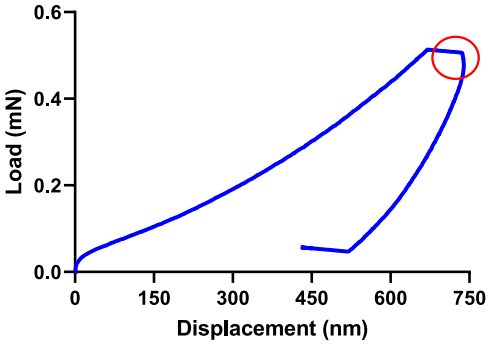

Figure 2. Nanoindentation load−displacement curve for the P3HT film subjected to the Oliver−Pharr method.

load−displacement curve of P3HT, which exhibits a time-dependent response. This is seen through continued deformation at a constant load and the "nose" or negative slope observed during the initial unloading phase.[42] The nanoindenter tip's modulus and Poisson's ratio were input as 1141 GPa and 0.07, respectively.[43] P3HT's Poisson's ratio was assumed to be 0.35, in accordance with values reported in the literature.[44] The Young's modulus determined from this analysis was 1.0 GPa, which is overestimated from the consensus by a factor of roughly four.

3.3. Nanoindentation by Viscoelastic Analysis. In contrast to the Oliver−Pharr technique, which utilizes the unloading portion of a load−displacement curve, the viscoelastic method analyzes the loading portion of the curve under a ramp-loading history. For a step-loading history, only the constant load section is considered. In accordance, Figure 3 shows the load−displacement curves of ramp-loading experiments. The material's response to loading at rates between 0.05 and 0.20 mN/s is essentially identical. Upon reaching an order of magnitude of difference, the response begins to change, which is common for viscoelastic materials. Strain rate dependence arises from the material possessing both viscous and elastic components, leading to higher strain rates yielding a stiffer material. As previously mentioned, nanoindentation data at very small depths are generally inaccurate, and thus, creep compliance is not calculated for penetration depths of less than 125 nm. Additionally, to avoid the substrate effect, analysis is limited to less than 10% of the film thickness. The load−displacement curves are fit to eq 5 by a nonlinear least squares

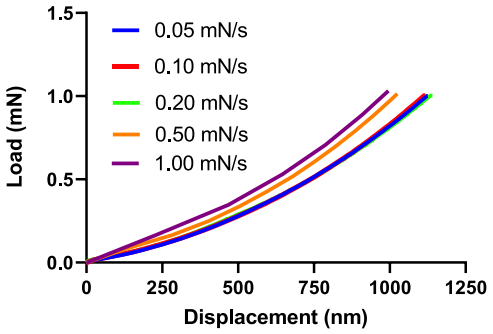

Figure 3. Nanoindentation load−displacement curves at different loading rates. Curves for loading rates 0.05, 0.10, and 0.20 mN/s are nearly overlapping with each other.

fitting technique (R^2 > 0.9999) by selecting values for the retardation times, τ_i (i = 1,2,3,4).

From this, shear creep compliance functions in the Prony series form in eq 6 are formed. Figure 4 depicts the shear creep compliance as a function of time, and Table 2 summarizes the compliance coefficients.

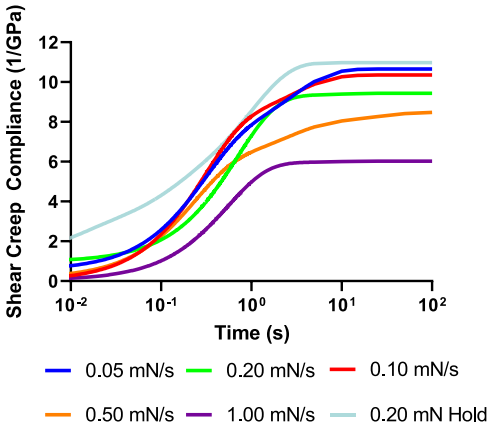

Figure 4. Shear creep compliance as a function of time.

Table 2. Compliance Coefficients

loading rate	J_o (GPa^{-1})	J_1 (GPa^{-1})	J_2 (GPa^{-1})	J_3 (GPa^{-1})
0.05 mN/s	0.536	6.35	3.77	0.195
0.10 mN/s	1.30×10^{-8}	7.77	2.58	0.220
0.20 mN/s	0.965	8.30	0.174	6.80×10^{-19}
0.50 mN/s	0.128	5.65	2.06	0.642
1.0 mN/s	0.0907	6.33	0.113	4.60×10^{-11}
0.20 mN hold	0.968	1.52	1.88	6.61

As the loading rate increases, the long-term values of the creep compliance functions decrease. In time-dependent materials, this is viewed as a loss of ductility accompanied by a lessened ability to absorb energy prior to a mechanical failure.[45,46] This may result in the material being more prone to permanent deformations like fractures under high-stress loading conditions.

The creep functions are next converted to relaxation functions in the form of eq 7 through a numerical interconversion in which the same approach and MATLAB code were used as reported by Luk-Cyr et al.[47] The parameters listed in Tables 1 and 2 stem from using the curve fitting approach to generate a Prony series and are associated with the

https://doi.org/10.1021/acsapm.3c00939
ACS Appl. Polym. Mater. 2023, 5, 6318−6324

time-dependent response of a specific polymer. When a desirable fit is achieved, the magnitudes are assumed to correspond to a physical relaxation and/or time-dependent response based on the corresponding time that was selected. Figure 5 gives a plot of the shear relaxation modulus over time.

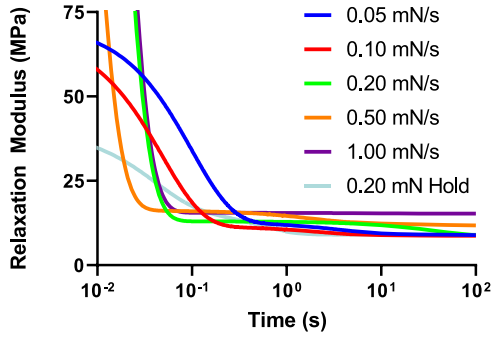

Figure 5. Shear relaxation modulus as a function of time.

Table 3 lists the relaxation coefficients and relaxation times. There is a large discrepancy of the initial shear relaxation modulus at loading rates above 0.10 mN/s. At faster loading rates, there is less time for the material to relax and dissipate energy in response to the applied load, which elicits a response to loading that is more stiff.[46] In general, P3HT exhibits rapid relaxation within the first half second before converging to an equilibrium value. The shear relaxation modulus converges to its equilibrium value for almost all indentations within 5 s. This equilibrium is mainly consistent for loading rates between 0.05 and 0.20 mN/s. Upon reaching faster loading rates, i.e., 0.50 and 1.00 mN/s, the relaxation modulus rapidly increases. The increase in the relaxation modulus is representative of the material experiencing an escalation in rigidity and greater resistance toward shear deformation at higher loading rates.[48,49]

Utilizing the shear relaxation modulus obtained in eq 7, we convert to Young's relaxation modulus through eq 8 for each loading rate and the step-loading test. Upon obtaining Young's relaxation modulus, a conversion was employed to obtain Young's modulus through eq 9. The average relaxation modulus over time in a load-controlled test for a given strain rate is equivalent to Young's modulus, which is determined by tensile testing or the buckling method. The results for Young's modulus at different loading rates as well as the average value from literature are plotted in Figure 6.[21−25] Overall, we obtain an average Young's modulus of 260 ± 27 MPa for loading rates below 0.50 mN/s. As the loading rate increases, there is an increase in the modulus, signifying an increase in material stiffness during fast loading cycles. This is also evident in the load−displacement curves, where the total penetration depth decreases at higher loading rates, despite the maximum load being consistent between experiments. These observations are consistent with those made in time-dependent materials due to the viscous component of their constitution. At lower strain rates, deformation occurs in a slow enough manner that there is an internal rearrangement of polymer chains that allow for the dissipation of energy. When the strain rate increases, a more rapid deformation occurs, and the material's rearrangement is not as effective.[45,50,51] This leads to energy being stored in an elastic manner, which is seen by an increase in stiffness.

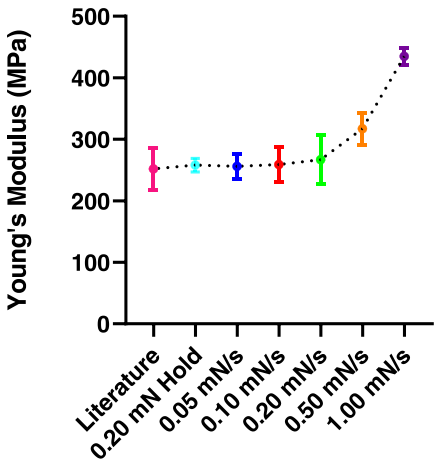

Figure 6. Young's modulus at different loading rates.

4. CONCLUSIONS

The nanoscale mechanical properties of P3HT were determined through a viscoelastic nanoindentation technique utilizing a Berkovich indenter. This method is necessary for accurate mechanical property characterization as polymers exhibit time-dependent responses to loading. Through the determination of viscoelastic properties such as the shear creep compliance and shear relaxation modulus and Young's relaxation modulus, Young's modulus was obtained at various loading rates. The data collected are in excellent agreement with values reported from specialized mechanical tests performed on P3HT thin films (20−200 nm thick). This is in stark contrast to those values reported in previous nanoindentation studies of P3HT, where the modulus values span over two orders of magnitude of difference. This viscoelastic analysis technique is more appropriate than the Oliver−Pharr method for the characterization of organic semiconductors as it accounts for time dependency in regard to applied stress. Oliver−Pharr is a simpler model with faster data analysis but leads to an overestimation of Young's modulus as the technique's governing model does not account for a polymer's time-dependent response. By considering viscoelastic effects, the error in the determination of Young's

Table 3. Relaxation Coefficients and Relaxation Times

loading rate	G_∞ (GPa)	G_1 (GPa)	G_2 (GPa)	G_3 (GPa)	λ_1 (s)	λ_2 (s)	λ_3 (s)
0.05 mN/s	0.0888	0.588	0.0348	3.70×10^{-3}	10.11	0.274	0.0201
0.10 mN/s	0.0871	0.570	0.0259	2.3×10^{-3}	20.6	0.473	0.0367
0.20 mN/s	0.0848	8.35	3.00×10^{-3}	0.0241	104	0.164	0.0241
0.50 mN/s	0.118	7.65	0.0350	8.90×10^{-3}	208	0.584	0.0350
1.00 mN/s	0.153	10.9	2.20×10^{-3}	1.43×10^{-11}	109	0.156	0.0154
0.20 mN hold	0.0905	6.54	0.233	2.08	1.44×10^{-3}	25.6	2.08

https://doi.org/10.1021/acsapm.3c00939
ACS Appl. Polym. Mater. 2023, 5, 6318−6324

modulus is minimized. This method shows promise in the determination of mechanical properties of other organic semiconducting materials.

■ ASSOCIATED CONTENT

Supporting Information

The Supporting Information is available free of charge at https://pubs.acs.org/doi/10.1021/acsapm.3c00939.

Detailed synthetic procedure for P3HT; ^{1}H NMR spectra of intermediate compounds and P3HT; absolute molecular weight determination by ^{1}H NMR; NMR and SEC characterization of P3HT; thermal characterization of P3HT; thin film optimization strategy; TMAFM images of optimized thin films; SEM image of Berkovich indenter tip; optical micrograph of residual impressions; fused silica calibration; reported values of Young's modulus (PDF)

■ AUTHOR INFORMATION

Corresponding Author

Mihaela C. Stefan − *Department of Chemistry and Biochemistry, School of Natural Sciences and Mathematics, The University of Texas at Dallas, Richardson, Texas 75080, United States;* orcid.org/0000-0003-2475-4635; Email: Mihaela@UTDallas.edu

Authors

Branston E. Mefferd − *Department of Chemistry and Biochemistry, School of Natural Sciences and Mathematics, The University of Texas at Dallas, Richardson, Texas 75080, United States*

Visakhan V. Nambiar − *Department of Mechanical Engineering, Erik Jonsson School of Engineering and Computer Science, The University of Texas at Dallas, Richardson, Texas 75080, United States*

Hongbing Lu − *Department of Mechanical Engineering, Erik Jonsson School of Engineering and Computer Science, The University of Texas at Dallas, Richardson, Texas 75080, United States;* orcid.org/0000-0003-4268-7245

Complete contact information is available at: https://pubs.acs.org/10.1021/acsapm.3c00939

Author Contributions

The manuscript was written with contributions from all authors. Each author has approved the final version of the manuscript.

Notes

The authors declare no competing financial interest.

■ ACKNOWLEDGMENTS

Financial support provided by the National Science Foundation (CHE-1609880 and CHE-1566059) and Welch Foundation (AT1740) is gratefully acknowledged. M.C.S. thanks the generous endowed chair support from the Eugene McDermott Foundation. We also acknowledge the support of the National Science Foundation under CMMI-2219347, Department of Energy under DE-NA0003962 and DE-NA0003525, SRC through TxACE under Task 2810.056. H.L. thanks the Louis A. Beecherl Jr., endowed Chair support.

■ REFERENCES

(1) Lee, J.; Park, S. A.; Ryu, S. U.; Chung, D.; Park, T.; Son, S. Y. Green-Solvent-Processable Organic Semiconductors and Future Directions for Advanced Organic Electronics. *J. Matter Chem. A* **2020**, *8*, 21455−21473.

(2) Kim, T.; Kim, J.-H.; Kang, T. E.; Lee, C.; Kang, H.; Shin, M.; Wang, C.; Ma, B.; Jeong, U.; Kim, T.-S.; Kim, B. J. Flexible, Highly Efficient All-Polymer Solar Cells. *Nat. Commun.* **2015**, *6*, No. 8547.

(3) Liu, F.; Hou, X.; Hu, B.; Li, R. Intrinsically Elastic Organic Semiconductors. *Molecules* **2021**, *26*, 6130−6142.

(4) Yang, Y.; Zhang, Z.; Bin, H.; Chen, S.; Gao, L.; Xue, L.; Yanh, C.; Li, Y. Side-Chain Isomerization on an n-Type Organic Semiconductor ITIC Acceptor Makes 11.77% High Efficiency Polymer Solar Cells. *J. Am. Chem. Soc.* **2016**, *138*, 15011−15018.

(5) Root, S. E.; Savagatrup, S.; Printz, A. D.; Rodriquez, D.; Lipomi, D. J. Mechanical Properties of Organic Semiconductors for Stretchable, Highly Flexible, and Mechanically Robust Electronics. *Chem. Rev.* **2017**, *117*, 6467−6499.

(6) Qian, Y.; Zhang, X.; Xie, L.; Qi, D.; Chandran, B. K.; Chen, X.; Huang, W. Stretchable Organic Semiconductor Devices. *Adv. Mater.* **2016**, *28*, 9243−9265.

(7) Savagatrup, S.; Printz, A. D.; O'Connor, T. F.; Zaretski, A. V.; Rodriquez, D.; Sawyer, E. J.; Rajan, K. M.; Acosta, R. I.; Root, S. E.; Lipomi, D. J. Mechanical Degredations and Stability of Organic Solar Cells: Molecular and Microstructural Determinants. *Energy Environ. Sci.* **2015**, *8*, 55−80.

(8) Wang, S.; Peng, L.; Sun, H.; Huang, W. The Future of Solution Processing Toward Organic Semiconductor Devices: a Substrate and Integration Perspective. *J. Mater. Chem. C.* **2022**, *10*, 12468−12486.

(9) Vinci, R. P.; Vlassak, J. J. Mechanical Behavior of Thin Films. *Annu. Rev. Matter. Sci.* **1996**, *26*, 431−462.

(10) Oliver, W. C.; Pharr, G. M. An Improved Technique for Determining Hardness and Elastic Modulus Using Load and Displacement Sensing Indentation Experiments. *J. Mater. Res.* **1992**, *7*, 1564−1583.

(11) Doerner, M. F.; Nix, W. D. A Method for Interpreting the Data from Depth-Sensing Indentation Instruments. *J. Mater. Res.* **1986**, *1*, 601−609.

(12) Sánchez, J.; El-Mansy, S.; Sun, B.; Scherban, T.; Fang, N.; Pantuso, D.; Ford, W.; Elizalde, M. R.; Martinez-Esnaola, J. M.; Martin-Meizoso, A.; Gil-Sevillano, J.; Fuentes, M.; Maiz, J. Cross-Sectional Nanoindentation: a New Technique for Thin Film Interfacial Adhesion Characterization. *Acta Mater.* **1999**, *47*, 4405−4413.

(13) Heinrich, C.; Waas, A. M.; Wineman, A. S. Determination of Material Properties Using Nanoindentation and Multiple Indenter Tips. *Int. J. Solids Struct.* **2009**, *46*, 364−376.

(14) Youssef, G. General Properties of Polymers. In *Applied Mechanics of Polymers*, 1st ed.; Elsevier, 2021; pp 19−48.

(15) Lu, H.; Wang, B.; Ma, J.; Huang, G.; Viswanathan, H. Measurement of Creep Compliance of Solid Polymers by Nano-indentation. *Mech. Time-Depend. Mater.* **2003**, *7*, 189−207.

(16) Li, H.-C.; Rao, K. K.; Jeng, J.; Hsiao, Y.; Guo, T.; Jeng, Y.; Wen, T. Nano-scale Mechanical Properties of Polymer/Fullerene Bulk Hetero-junction Films and Their Influence on Photovoltaic Cells. *Sol. Energy Mater. Sol. Cells* **2011**, *95*, 2976−2980.

(17) Nanayakkara, M. P. A.; Masteghin, M. G.; Basirico, L.; Fratelli, I.; Ciavatti, A.; Kilbride, R. C.; Jenatsch, S.; Webb, T.; Richheimer, F.; Wood, S.; Castro, F. A.; Parnell, A. J.; Fraboni, B.; et al. Molecular Weight Tuning of Organic Semiconductors for Curved Organic-Inorganic Hybrid X-Ray Detectors. *Adv. Sci.* **2022**, *9*, No. 2101746.

(18) Pulliam, E.; Hoover, G.; Tiparti, D.; Ryu, D.Development of Self-Powered Strain Sensor Using Mechano-Luminescent ZnS:Cu and Mechano-Optoelectronic P3HT. In *Sensors and Smart Structures Technologies for Civil, Mechanical, and Aerospace Systems*; SPIE, 2017; Vol. *10168*, pp 88−102.

(19) Gao, L.; Tian, Y. M.; Hou, W.; Yan, W. Q.; Zhong, G. Y. Piezoresisitance of Poly(3-Hexylthiophene) Film. *Adv. Polym. Technol.* **2018**, *37*, 662−667.

(20) An, X.; Wang, K.; Bai, L.; Wei, C.; Xu, M.; Yu, M.; Han, Y.; Sun, N.; Sun, L.; Lin, J.; Ding, X.; Xie, L.; Zhang, Q.; Qin, T.; Huang, W. Intrinsic Mechanical Properties of the Polymeric Semiconductors. *J. Mater. Chem. C* **2020**, *8*, 11631−11637.
(21) Kim, J.-S.; Kim, J.-H.; Lee, W.; Yu, H.; Kim, H. J.; Song, I.; Shin, M.; Oh, J. K.; Jeong, U.; Kim, T.; Kim, B. J. Tuning Mechanical and Optoelectrical Properties of Poly(3-hexylthiophene) Through Systematic Regioregularity Control. *Macromolecules* **2015**, *48*, 4339−4346.
(22) Rodriquez, D.; Kim, J.-H.; Root, S. E.; Fei, Z.; Boufflet, P.; Heeney, M.; Kim, T.-S.; Lipomi, D. J. Comparison of the Methods for Determining the Mechanical Properties of Semiconducting Polymer Films for Stretchable Electronics. *ACS Appl. Mater. Interfaces* **2017**, *9*, 8855−8862.
(23) O'Connor, B.; Chan, E. P.; Chan, C.; Conrad, B. R.; Richter, L. J.; Kline, R. J.; Heeney, M.; McCulloch, I.; Soles, C. L.; DeLongchamp, D. M. Correlations Between Mechanical and Electrical Properties of Polythiophenes. *ACS Nano* **2010**, *4*, 7538−7544.
(24) Awartani, O. A.; Lemanski, B. I.; Ro, H. W.; Richter, L. J.; DeLongchamp, D. M.; O'Connor, B. T. Correlating Stiffness, Ductility, and Morphology of Polymer: Fullerene Films for Solar Cell Applications. *Adv. Energy Mater.* **2013**, *3*, 399−406.
(25) Zhang, S.; Ocheje, M. U.; Luo, S.; Ehlenberg, D.; Appleby, B.; Weller, D.; Zhou, D.; Gagne-Rondeau, S.; Gu, X. Probing the Viscoelastic Property of Pseudo Free-Standing Conjugated Polymeric Thing Films. *Macromol. Rapid Commun.* **2018**, *39*, No. 1800092.
(26) Tahk, D.; Lee, H. H.; Khang, D.-Y. Elastic Moduli of Organic Electronic Materials by the Buckling Method. *Macromolecules* **2009**, *42*, 7079−7083.
(27) Lee, E. H.; Radok, J. R. M. The Contact Problem for Viscoelastic Bodies. *J. Appl. Mech.* **1960**, *27*, 438−444.
(28) Luo, H.; Zhang, Y.; Wang, B.; Lu, H. Characterization of the Compressive Behavior of Glass Fiber Reinforced Polyurethane Foam at Different Strain Rates. *J. Offshore Mech. Arct. Eng.* **2010**, *132*, No. 021301.
(29) Xu, T.; Yoo, J. H.; Babu, S.; Roy, S.; Lee, J.-B.; Lu, H. Characterization of the Mechanical Behavior of SU-8 at Microscale by Viscoelastic Analysis. *J. Micromech.Microeng.* **2016**, *26*, No. 105001.
(30) Lohwasser, R. H.; Thelakkat, M. Toward Perfect Control of End Groups and Polydispersity in Poly(3-hexylthiophene) via Catalyst Transfer Polymerization. *Macromolecules* **2011**, *44*, 3388−3397.
(31) Iovu, M. C.; Sheina, E. E.; Gil, R. R.; McCullough, R. D. Experimental Evidence for the Quasi-"Living" Nature of the Grignard Metathesis Method for the Synthesis of Regioregular Poly(3-hexylthiophenes). *Macromolecules* **2005**, *38*, 8649−8656.
(32) Jiang, W.-G.; Su, J.-J.; Feng, X.-Q. Effect of Surface Roughness on Nanoindentation Test of Thin Films. *Eng. Fract. Mech.* **2008**, *75*, 4965−4972.
(33) Bolshakakov, A. P.; Pharr, G. M. Influences of Pileup on the Measurement of Mechanical Properties by Load and Depth Sensing Indentation Technique. *J. Mater. Res.* **1998**, *13*, 1049−1058.
(34) Hardiman, M.; Vaughn, T. J.; McCarthy, C. T. The Effects of Pile-Up, Viscoelasticity and Hydrostatic Stress on Polymer Matrix Nanoindentation. *Polym. Test.* **2016**, *52*, 157−166.
(35) Saha, R.; Nix, W. D. Effects of the Substrate on the Determination of Thin Film Mechanical Properties by Nano-indentation. *Acta Mater.* **2002**, *50*, 23−38.
(36) Pei, D.; Wang, Z.; Peng, Z.; Zhang, J.; Deng, Y.; Han, Y.; Ye, L.; Geng, Y. Impact of Molecular Weight on the Mechanical and Electrical Properties of a High-Mobility Diketopyrrolopyrrole-Based Conjugated Polymer. *Macromolecules* **2020**, *53*, 4490−4500.
(37) Abbasi, M.; Pokhrel, D.; Coats, E. R.; Guho, N. M.; McDonald, A. G. Effect of 3-Hydroxyvalerate Content of Thermal, Mechanical, and Rheological Properties of Poly(3-hydroxybutyrate-co-3-hydroxyvalerate) Biopolymers Produced from Fermented Dairy Manure. *Polymers* **2022**, *14*, 4140.
(38) Sista, P.; Wilson, M.; Holmes, N.; Kularatne, R. S.; Rainbolt, E. A.; Biewer, M. C.; Dastoor, P. C.; Belcher, W.; Stefan, M. C. Non-Dependence of Polymer to PCBM Weight Ratio on the Performance of Bulk Heterojunction Solar Cells with Benzodithiophene Donor Polymer. *Sci. Adv. Mater.* **2013**, *5*, 512−518.
(39) Dissanayake, D. S.; Sheina, E.; Biewer, M. C.; McCullough, R. D.; Stefan, M. C. Determination of Absolute Molecular Weight of Regioregular Poly(3-hexylthiophene) by 1H-NMR Analysis. *J. Polym. Sci., Part A: Polym. Chem.* **2017**, *55*, 79−82.
(40) Pascui, O. F.; Lohwasser, R.; Sommer, M.; Thelakkat, M.; Thrun-Albrecht, T.; Saalwachter, K. High Crystallinity and Nature of Crystal-Crystal Phase Transformations in Regioregular Poly(3-hexylthiophene). *Macromolecules* **2010**, *43*, 9401−9410.
(41) Kohn, P.; Huettner, S.; Komber, H.; Senkovsky, V.; Tkachov, R.; Kiriy, A.; Friend, R. H.; Steiner, U.; Huck, W. T. S.; Sommer, S.-U.; Sommer, M. On the Role of Single Regiodefects and Polydispersity in Regioregular Poly(3-hexylthiophene): Defect Distribution, Synthesis of Defect-Free Chains, and a Simple Model for the Determination of Crystallinity. *J. Am. Chem. Soc.* **2012**, *134*, 4790−4805.
(42) Ngan, A. H. W.; Tang, B. Viscoelastic Effects During Unloading in Depth-Sensing Indentation. *J. Mater. Res.* **2002**, *17*, 2604−2610.
(43) Gao, C.; Liu, M. Instrumented Indentation of Fused Silica by Berkovich Indenter. *J. Non-Cryst. Solids* **2017**, *475*, 151−160.
(44) Root, S. E.; Savagatrup, S. S.; Pais, J. P.; Arya, G.; Lipomi, D. J. Predicting the Mechanical Properties of Organic Semiconductors Using Coarse-Grained Molecular Dynamics Simulations. *Macromolecules* **2016**, *49*, 2886−2894.
(45) Khieng, T. K.; Debnath, S.; Liang, E. T. C.; Anwar, M.; Pramanik, A.; Basak, A. K. A Review on Mechanical Properties of Natural Fibre Reinforced Polymer Composites under Various Strain Rates. *J. Compos. Sci.* **2021**, *5*, 130−143.
(46) Lejeune, J.; Houerou, V. L.; Chatel, T.; Pelletier, H.; Gauthier, C.; Mulhaupt, R. Creep and Recovery Analysis of Polymeric Materials During Indentation Tests. *Eur. J. Mech., A Solids* **2018**, *68*, 1−8.
(47) Luk-Cyr, J.; Crochon, T.; Li, C.; Lévesque, M. Interconversion of Linearly Viscoelastic Material Functions Expressed as a Prony Series: A Closure. *Mech. Time-Depend. Mater.* **2013**, *17*, 53−82.
(48) Dwivedi, K. K.; Lakhani, P.; Kumar, S.; Kumar, N. The Effect of Strain Rate on the Stress Relaxation of the Pig Dermis: A Hyper-Viscoelastic Approach. *J. Biomech. Eng.* **2020**, *142*, No. 091006.
(49) Brinson, H. F.; Brinson, L. C. Time-Temperature Superposition and Rate Effects. In *Polymer Engineering Science and Viscoelasticity: An Introduction*; Springer Science & Business Media: New York, 2008; pp 187−223.
(50) Obaid, N.; Kortschot, M. T.; Mohini, S. Understanding the Stress Relaxation Behavior of Polymers Reinforced with Short Elastic Fibers. *Materials* **2017**, *10*, 472−487.
(51) Wang, C.; Akbulatov, S.; Chen, Q.; Tian, Y.; Sun, C.-L.; Couty, M.; Boulatov, R. The Molecular Mechanism of a Mechanically-Loaded Polymer. *Nat. Commun.* **2022**, *13*, No. 3154.

https://doi.org/10.1021/acsapm.3c00939
ACS Appl. Polym. Mater. 2023, 5, 6318−6324